

RESEARCH ARTICLE

10.1002/2013JD020138

Key Points:

- Dynamic response to volcanic eruption depends on the ozone concentrations
- Stronger ozone gradients strengthen the dynamic response
- Resulting winter warming pattern is highly significant

Supporting Information:

- Readme
- Figure S1
- Figure S2
- Figure S3
- Figure S4

Correspondence to:

S. Muthers,
muthers@climate.unibe.ch

Citation:

Muthers, S., J. G. Anet, C. C. Raible, S. Brönnimann, E. Rozanov, F. Arfeuille, T. Peter, A. I. Shapiro, J. Beer, F. Steinhilber, Y. Brugnara, and W. Schmutz (2014), Northern hemispheric winter warming pattern after tropical volcanic eruptions: Sensitivity to the ozone climatology, *J. Geophys. Res. Atmos.*, 119, 1340–1355, doi:10.1002/2013JD020138.

Received 8 MAY 2013

Accepted 14 JAN 2014

Accepted article online 18 JAN 2014

Published online 15 FEB 2014

Northern hemispheric winter warming pattern after tropical volcanic eruptions: Sensitivity to the ozone climatology

S. Muthers^{1,2}, J. G. Anet³, C. C. Raible^{1,2}, S. Brönnimann^{2,4}, E. Rozanov^{3,5}, F. Arfeuille^{2,4}, T. Peter³, A. I. Shapiro⁵, J. Beer⁶, F. Steinhilber⁶, Y. Brugnara^{2,4}, and W. Schmutz⁵

¹Climate and Environmental Physics, University of Bern, Bern, Switzerland, ²Oeschger Centre for Climate Change Research, University of Bern, Bern, Switzerland, ³Institute for Atmospheric and Climate Science, ETH, Zurich, Switzerland, ⁴Institute of Geography, University of Bern, Bern, Switzerland, ⁵Physikalisch-Meteorologisches Observatorium Davos and World Radiation Center, Davos, Switzerland, ⁶Swiss Federal Institute of Aquatic Science and Technology, Dübendorf, Switzerland

Abstract An important key for the understanding of the dynamic response to large tropical volcanic eruptions is the warming of the tropical lower stratosphere and the concomitant intensification of the polar vortices. Although this mechanism is reproduced by most general circulation models today, most models still fail in producing an appropriate winter warming pattern in the Northern Hemisphere. In this study ensemble sensitivity experiments were carried out with a coupled atmosphere-ocean model to assess the influence of different ozone climatologies on the atmospheric dynamics and in particular on the northern hemispheric winter warming. The ensemble experiments were perturbed by a single Tambora-like eruption. Larger meridional gradients in the lower stratospheric ozone favor the coupling of zonal wind anomalies between the stratosphere and the troposphere after the eruption. The associated sea level pressure, temperature, and precipitation patterns are more pronounced and the northern hemispheric winter warming is highly significant. Conversely, weaker meridional ozone gradients lead to a weaker response of the winter warming and the associated patterns. The differences in the number of stratosphere-troposphere coupling events between the ensembles experiments indicate a nonlinear response behavior of the dynamics with respect to the ozone and the volcanic forcing.

1. Introduction

Large tropical volcanic eruptions are a major factor in natural climate change [Robock, 2000; Cole-Dai, 2010; Timmreck, 2012]. The direct radiative effect of an eruption leads to a cooling at the surface. At the same time, dynamic effects can cause positive temperature anomalies on the regional scale, e.g., in the Northern Hemisphere where a winter warming pattern has been identified at high latitudes after several historical eruptions [e.g., Robock and Mao, 1992; Stenchikov et al., 2002; Shindell et al., 2004; Fischer et al., 2007; Christiansen, 2008; Zanchettin et al., 2012]. After the eruption of Mount Pinatubo in 1991 climate model simulations indicated that the winter warming following the eruption is related to stratospheric dynamics [Graf et al., 1993]. The aerosol loading in the lower stratosphere increases the reflection of short-wave radiation back to space and the absorption of near-infrared and long-wave radiation. For tropical and subtropical volcanic eruptions a large fraction of the aerosol is advected into the tropical pipe, so that its long-wave absorption leads to a warming of the tropical stratosphere, which strengthens the meridional temperature gradient and accelerates the polar night jet [Kodera, 1994]. These wind anomalies penetrate downward into the troposphere and intensify the westerlies [Graf et al., 1993]. Therefore, the radiative forcing of the volcanic eruption can induce a positive phase of the Arctic Oscillation (AO) or the North Atlantic Oscillation (NAO), which is held responsible for the higher winter temperature in the northern high latitudes [Robock, 2000; Shindell et al., 2004].

A number of mechanisms was proposed to explain the propagation of wind anomalies from the stratosphere to the troposphere or vice versa [Shepherd, 2002; Song and Robinson, 2004]. However, none of them is yet fully understood [Thompson et al., 2006; Gerber et al., 2012]. Alternatively, several studies described the interaction between stratosphere and troposphere in a statistical way using empirical orthogonal function analysis or correlations techniques [e.g., Baldwin et al., 1994; Baldwin and Dunkerton, 2001; Thompson et al., 2005]. These authors defined stratosphere-troposphere couplings by coupled modes of variability between the stratosphere and the troposphere. For the Northern Hemisphere this coupled mode

consists of the stratospheric polar vortex and the NAO or AO. Independent of the underlying mechanisms, stratosphere-troposphere coupling is known to be the key to understanding the winter warming pattern that follows large volcanic eruptions.

The state of the stratosphere has significantly changed in the past few decades. In particular, its composition has changed due to increased anthropogenic emissions of greenhouse gases, aerosol, and ozone-depleting substances [Solomon, 1999; Baldwin *et al.*, 2007]. The temperature changes, resulting from this change in composition, alter the stratospheric dynamics [Gillett *et al.*, 2002; Gillett and Thompson, 2003; Thompson *et al.*, 2011] and might influence the response of the circulation to volcanic eruption, though the magnitude of the temperature changes is still under discussion [Thompson *et al.*, 2012].

Moreover, the dynamic response of the atmosphere to a strong volcanic eruption also depends on the direct effects of the eruption products on the stratospheric chemistry. In modern times, i.e., in the presence of ozone-depleting halogens, sulfate aerosols act as a component to facilitate heterogeneous reactions, which deactivate nitrogen oxides (NO_x), but in turn activate halogens, leading to a significant reduction of the ozone concentrations [Solomon, 1999; Rozanov *et al.*, 2002]. In preindustrial times with low halogen loading in the stratosphere, the ozone mixing ratios increase after powerful volcanic eruptions, due to heterogeneous deactivation reactions of NO_x on the sulfate aerosol surfaces, slowing down the NO_x -driven ozone destruction cycles [Tie and Brasseur, 1995; Solomon *et al.*, 1996].

For the Pinatubo eruption Stenchikov *et al.* [2002] simulated the impact of the ozone depletion on the temperatures and the dynamics using the SKYHI model forced by observed ozone anomalies. They estimated the cooling to be in the order of 1 K in the tropics and more than 6 K in the northern polar stratosphere. The high-latitude cooling increases the meridional temperature gradient and produces a positive phase of the AO.

The ability of general circulation models (GCMs) to simulate the dynamically induced winter warming in the Northern Hemisphere was evaluated in several studies [Stenchikov *et al.*, 2006; Miller *et al.*, 2006; Driscoll *et al.*, 2012]. For the Intergovernmental Panel on Climate Change Fourth Assessment Report (IPCC AR4) models, Stenchikov *et al.* [2006] revealed that some of the models tend to simulate positive AO phases, but the amplitude was in general too weak compared to observations. Furthermore, models may underestimate the stratospheric-troposphere coupling [Miller *et al.*, 2006]. For the Coupled Model Intercomparison Project Phase 5 (CMIP5) [Taylor *et al.*, 2012], Driscoll *et al.* [2012] repeated the evaluation of Stenchikov *et al.* [2006]. Despite improvements in spatial resolution and representation of the aerosol forcing, none of the 13 evaluated CMIP5 models was able to simulate a sufficiently strong dynamic response.

None of these evaluated CMIP3 and CMIP5 models included an interactive ozone chemistry module. To consider the radiative forcing of ozone in the radiation scheme ozone values are either prescribed in a constant or in a time-dependent way. Half of the IPCC AR4 models were forced by constant ozone climatologies [Miller *et al.*, 2006; Son *et al.*, 2010]. Depending on the climatology used the state of the stratosphere could differ and may influence the response to tropical eruptions.

The aim of this study is to analyze the role of different ozone climatologies in the dynamic response to tropical volcanic eruptions using a coupled atmosphere-ocean model simulation without interactive chemistry. In section 2 the setup of the simulations and the ozone climatologies are described; section 3 presents the results. In section 4 the results and the climatologies are discussed and compared to proxy data and other ozone data sets.

2. Model and Experiment Design

Our basic approach is to examine the dynamic response to tropical volcanic eruptions using two different background ozone climatologies applied to the coupled atmosphere-ocean model SOCOL3-MPIOM (Max Planck Institute ocean model).

SOCOL3 (Solar Climate Ozone Links, Stenke *et al.* [2013]) consists of the atmosphere model MA-ECHAM (middle atmosphere configuration) version 5.4.01 [Roeckner *et al.*, 2003] coupled to a modified version of the chemistry module MEZON (ModEl for investigation of the oZONe trends). In this study the interactive chemistry module is disabled as we focus on the role of background ozone level on the dynamic atmospheric response to large tropical eruptions. Still, SOCOL3 without interactive chemistry differs from the original

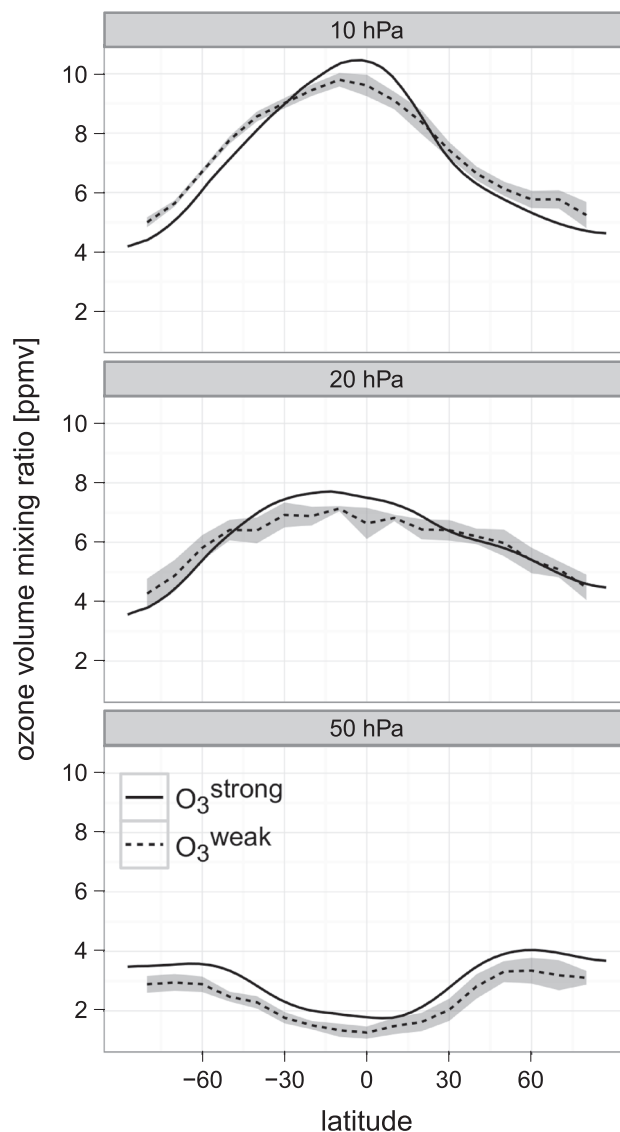


Figure 1. Mean winter season (December–January–February (DJF)) ozone mixing ratios in ppmv at 10, 20, and 50 hPa pressure altitudes of the two ozone climatologies used in this study. Dashed curve: climatology with weaker meridional gradient (O_3^{weak}) from Fortuin and Kelder [1998]. Shading: one standard deviation. Solid curve: climatology with stronger meridional gradient (O_3^{strong}) extracted from a 800 year long preindustrial control simulation with the interactive chemistry–climate model SOCOL3-MPIOM.

MA-ECHAM in several aspects (e.g., spectral solar irradiance forcing). For the experiments, a model resolution of T31 in the atmosphere (approximately $3.75^\circ \times 3.75^\circ$) and 39 vertical levels up to 0.01 hPa (80 km) is used.

The ocean model MPIOM (Max Planck Institute ocean model [Marsland, 2003; Jungclaus *et al.*, 2006]) is used in a nominal resolution of 3° , but with the North Pole shifted toward Greenland, to reach higher resolution in the North Atlantic and in the deepwater formation regions. Both components are coupled using the OASIS3 coupler [Budich *et al.*, 2010; Valcke, 2013].

Ozone Climatologies. Different states of the stratosphere are represented by two ozone climatologies, which are characterized by different meridional ozone gradients in the middle stratosphere. The first climatology is from Fortuin and Kelder [1998] and is based on observational data for the period 1980–1991. It is distributed with the ECHAM5 package and therefore used widely in ECHAM5 simulations [e.g., Jungclaus *et al.*, 2010]. The second climatology was extracted from a 800 year long preindustrial control simulation for 1600 A.D. conditions with the interactive chemistry–climate model SOCOL3-MPIOM by averaging over the last 400 simulation years assuming a nearly steady state. Both climatologies are zonally averaged and interpolated to

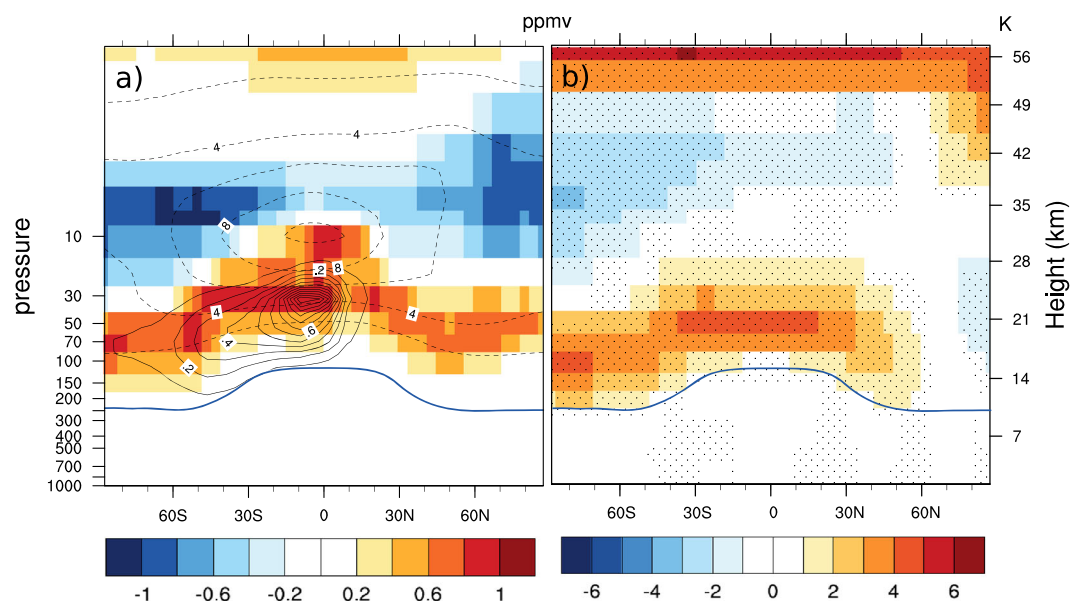


Figure 2. (a) Colored: Zonal mean seasonal mean (DJF) differences in the ozone volume mixing ratios (ppmv) between the two climatologies ($O_3^{\text{strong}} - O_3^{\text{weak}}$). Solid contours: volcanic aerosol forcing in terms of cumulative extinctions (from 0 to 1.5 km^{-1}) in the visible band of the model (440–690 nm) during the first year after the eruption. Dashed contours: mean DJF ozone volume mixing ratios (from 0 to 14 ppmv) in O_3^{strong} . (b) Resulting zonal average DJF temperature differences in K between the two control ensembles ($\text{CTRL}_{O_3^{\text{strong}}} - \text{CTRL}_{O_3^{\text{weak}}}$). Stippling: significant differences (Student's t test $p < 0.05$). Thick blue curve: DJF mean approximate tropopause height.

the same pressure levels. In Figure 1 the climatologies are compared for different levels in the stratosphere, and in Figure 2 a in terms of zonal mean anomalies. A general feature of ozone distributions (Figure 1) is that the meridional gradient is positive at low altitudes (i.e., more ozone toward the poles), but negative at high altitudes (i.e., more ozone toward the equator). This is caused by the enhanced ozone production in the tropical upper stratosphere relative to the midlatitude and higher latitude. The climatology of Fortuin and Kelder [1998] shows lower values below 30 hPa. Differences reach 20 % in the lower stratosphere, which is partly due to the fact that the Fortuin and Kelder [1998] climatology reflects the impact of industrial ozone-depleting species. Conversely, at altitudes above the 30 hPa level this climatology shows up to 10 % higher values of ozone, possibly due to the lower solar UV irradiance for the year 1600 climatology. For comparison the standard deviation of the Fortuin and Kelder [1998] climatology is shown as shading in Figure 1. At the three selected levels the difference between the two data sets are for most latitudes in the order of two standard deviations. For the dynamics in the stratosphere the meridional distribution of ozone is more important than its absolute value due to the thermal wind relationship. For the meridional gradient the largest differences between the two climatologies are found at the levels with the highest absolute mixing ratios, i.e., 1.3 ppmv between tropics and northern high latitudes around 10 hPa (Figure 1). Here the gradient is considerably weaker in the Fortuin and Kelder [1998] climatology. We therefore distinguish the two climatologies in terms of their meridional ozone gradient in the middle stratosphere and refer to them as O_3^{weak} (climatology of Fortuin and Kelder [1998]) and O_3^{strong} (model climatology).

Ensemble simulations. Two control ensemble experiments are performed forced by O_3^{strong} and O_3^{weak} , respectively. These two experiments $\text{CTRL}_{O_3^{\text{strong}}}$ and $\text{CTRL}_{O_3^{\text{weak}}}$ are used as reference. Except for the different ozone climatologies both control ensembles are driven with identical greenhouse gas and solar forcing, representing 1600 A.D. conditions.

Additionally, two sets of ensemble simulations are performed, with a tropical volcanic eruptions applied in the third year after the start of the simulations. Again, we use the strong gradient ozone climatology ($\text{VOLC}_{O_3^{\text{strong}}}$) and the weak gradient climatology ($\text{VOLC}_{O_3^{\text{weak}}}$). The simulation length of each ensemble member is 18 years. The ensemble names and configurations are summarized in Table 1.

For each set, 15 ensemble members are carried out using different initial conditions from a long-term control simulation. The restart files for the ocean, atmosphere, and the coupler were selected in 10 year steps,

Table 1. Overview of the Ensemble Simulations^a

Label	O ₃ Climatology	Volcanic Eruption
CTRL.O ₃ ^{strong}	O ₃ ^{strong}	No
VOLC.O ₃ ^{strong}	O ₃ ^{strong}	Yes
CTRL.O ₃ ^{weak}	O ₃ ^{weak}	No
VOLC.O ₃ ^{weak}	O ₃ ^{weak}	Yes

^aLabel: name used in this manuscript, O₃ climatology: ozone forcing, and indicator whether the members are perturbed by a volcanic eruption. Ensemble size is 15 for all ensembles, and each member ran for 18 years.

covering the period of year 500 to 640 in the long-term control. The large ensemble size increases the signal-to-noise ratio for the winter warming pattern [Shindell *et al.*, 2004] and allows to average out influences of El Niño–Southern Oscillation on the dynamic response to the eruption [Shindell *et al.*, 2004; Zhang *et al.*, 2012].

In the following the results from the perturbed ensemble sets are presented as anomalies to the unperturbed mean of the corresponding control ensemble. The mean of each control ensemble was calculated by averaging over all available simulation

years, i.e., 15 experiments × 18 years. As statistical test for the comparison we use an unpaired, two-sided Student’s *t* test [von Storch and Zwiers, 2000]. The degree of freedom defined in the test is 28 when comparing two perturbed ensembles (15 + 15 – 2) and 283 when comparing a perturbed ensemble and its corresponding control (15 × 18 + 15 – 2). The high number of degrees of freedom is possible due to the very low autocorrelation in the year-to-year DJF values.

Volcanic Forcing. The eruption used in the perturbed ensemble sets is the Tambora eruption that took place in April 1815 in Indonesia and led to the “year without a summer” [Stothers, 1984; Auchmann *et al.*, 2012]. The volcanic aerosol loading data set was prepared offline using the Atmospheric and Environmental Research Inc. model AER [Arfeuille *et al.*, 2013a]. As the transport of the aerosols in the stratosphere is directed mainly toward the winter hemisphere, the majority of aerosols is spread toward the Southern Hemisphere (compare to Figure 6 in Arfeuille *et al.* [2013a]). The cumulative extinction in the visible band (440–690 nm) for the first year of the eruption is shown as solid contours in Figure 2a. Figure 3 (left) displays the monthly mean aerosol optical depth in the visible band.

For the lower boundary over land, the land surface data of the ECHAM5 package is used [Hagemann, 2002]. In the highest levels of the equatorial stratosphere, the zonal winds are forced by data sets of the quasi-biennial oscillation (QBO). Here a backward extended version of the reconstruction of Brönnimann *et al.* [2007] was used for nudging the model. The QBO was in a westerly phase at the beginning of the eruption and shifted to an easterly phase in the following winter season. The QBO forcing is the same in the control and in the perturbed simulations, meaning that the QBO phase in the third year of each simulations is identical. However, climatological values for the control ensemble simulations are calculated using all available simulation years. In this case the influence of the QBO is averaged out.

Finally, we note that neither the ozone concentrations nor the volcanic aerosols are transported or else affected by the model but are prescribed according to the climatological or aerosol record data.

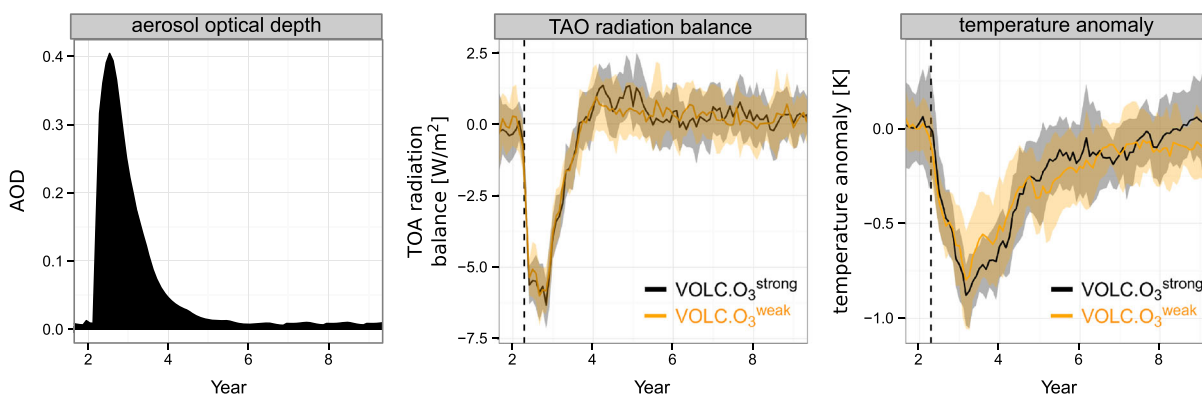


Figure 3. (left) Changes in the monthly mean optical depth at 550 nm caused by the volcanic eruption. (middle) Globally averaged monthly mean top-of-the-atmosphere (TOA) radiation balance anomalies relative to the average annual cycle in the corresponding control ensemble. (right) Monthly mean global mean temperature anomalies. Shading: ensemble standard deviation. Vertical dashed line: start of the eruption.

3. Results From the Sensitivity Experiments

3.1. Global Scale

We focus first on the global scale, where a surface cooling that follows the eruption is found in both perturbed ensemble simulations (VOLC.O₃^{strong} and VOLC.O₃^{weak}, compare Figure 3). The cooling is largest 1 year after the eruption with a reduction of the global average annual mean temperature of -0.75 K in VOLC.O₃^{strong} and -0.63 K in VOLC.O₃^{weak}, respectively. The differences between the ensemble mean VOLC.O₃^{strong} anomalies and the ensemble mean VOLC.O₃^{weak} anomalies are significant with $p = 0.037$ (Student's t test). The cooling is larger in the Southern Hemisphere due to the larger amount of aerosols in the southern stratosphere. Globally, the cooling is statistically significant for 6 years in VOLC.O₃^{strong} and for 7 years in VOLC.O₃^{weak} ($p < 0.05$, Student's t test). In terms of the top-of-the-atmosphere radiative forcing (Figure 3, middle) VOLC.O₃^{weak} experiences a maximum reduction of -6.0 W/m², whereas the reduction is slightly but insignificantly larger in VOLC.O₃^{strong} (-6.3 W/m²).

3.2. Regional Scale

The response for the northern hemispheric winter warming is shown in Figure 4 for the 2 m temperature, for the 500 hPa geopotential height, and for precipitation. In both ensemble experiments a temperature dipole with warming over northern and eastern Europe and cooling over southern Europe and the Middle East is identified. However, the warming of near-surface air over Scandinavia (2.7 K versus 1.0 K, area average between 10°E–30°E and 55°N–70°N, gray box in Figure 4) is considerably stronger and its significance higher in VOLC.O₃^{strong} than in VOLC.O₃^{weak}. Further temperature anomalies in VOLC.O₃^{strong} are a warming over eastern North-America and a cold anomaly over western Greenland and in the Labrador Sea. In VOLC.O₃^{weak} these cold anomalies are much weaker or missing.

The anomalies for both perturbed ensemble experiments are expressed relative to their corresponding control ensemble and the differences found between the two anomalies are therefore not related to differences between the control ensembles. The differences between the two control ensembles are shown in Figure S1a in the supporting information for the 2 m temperatures in winter (DJF, supporting information). In the two perturbed ensemble experiments the warming in northern Europe is related to an anomalously high 500 hPa geopotential height in the Atlantic basin located between 35°N and 55°N and low geopotential height west of Iceland, similar to a positive phase of the NAO. This pattern intensifies advection of warm Atlantic air masses toward Scandinavia. Similar to the temperature, the 500 hPa geopotential anomalies are largely significant over the Atlantic basin in VOLC.O₃^{strong}, but almost insignificant in VOLC.O₃^{weak}. The pattern of the sea level pressure anomalies are very similar illustrating the barotropic structure (Figure S2 in the supporting information). The differences in the sea level pressure between the two control ensemble experiment is shown in Figure S1b for the boreal winter season (DJF, supporting information). Clearly, the positive NAO-type pattern also shifts the storm track at the eastern boundary of the Atlantic basin toward the north and results in higher precipitation in northern Europe and less precipitation in southern Europe [Hurrell, 1995; Raible et al., 2004; Fischer et al., 2007; Pinto and Raible, 2012]. The precipitation anomalies are again highly significant in VOLC.O₃^{strong}, whereas they are insignificant in the VOLC.O₃^{weak} simulations.

3.3. Zonal Wind Changes

A possible explanation for this difference in the tropospheric dynamic lies in the behavior of the polar vortex and the stratosphere-troposphere coupling identified in the two ensemble experiments. An index for the strength of the polar vortex and the downward propagation of anomalies is the zonal mean zonal wind at 60°N [Christiansen, 2001, 2005] in the following named \bar{u}_{60} . Figure 5a displays the time series of \bar{u}_{60} at 10 hPa following the eruption. For comparison the mean annual cycle in the two control ensembles is shown as dashed lines. In the perturbed ensemble experiments an intensification of the wind speed starts a few months after the eruption. This intensification increases in winter and reaches its maximum in mid-February for VOLC.O₃^{weak} and by the end of February for VOLC.O₃^{strong}. Additionally, the vortex is significantly weakened in the VOLC.O₃^{weak} experiment by the end of December, whereas the vortex in VOLC.O₃^{strong} remains very strong throughout the winter. Moreover, the polar vortex is significantly stronger in VOLC.O₃^{strong} from February on ($p \leq 0.05$, Student's t test) than in the VOLC.O₃^{weak} experiment. The increase of the vortex speed relative to the respective control ensemble are comparable. This indicates that the additional intensification caused by the volcanic eruption is comparable for both ozone climatologies.

We also find a clear difference in the vortex intensities between the control ensembles (dashed lines in Figure 5a). In January, when the vortex index reaches its maximum, zonal winds are about 5 m/s ($\sim 15\%$)

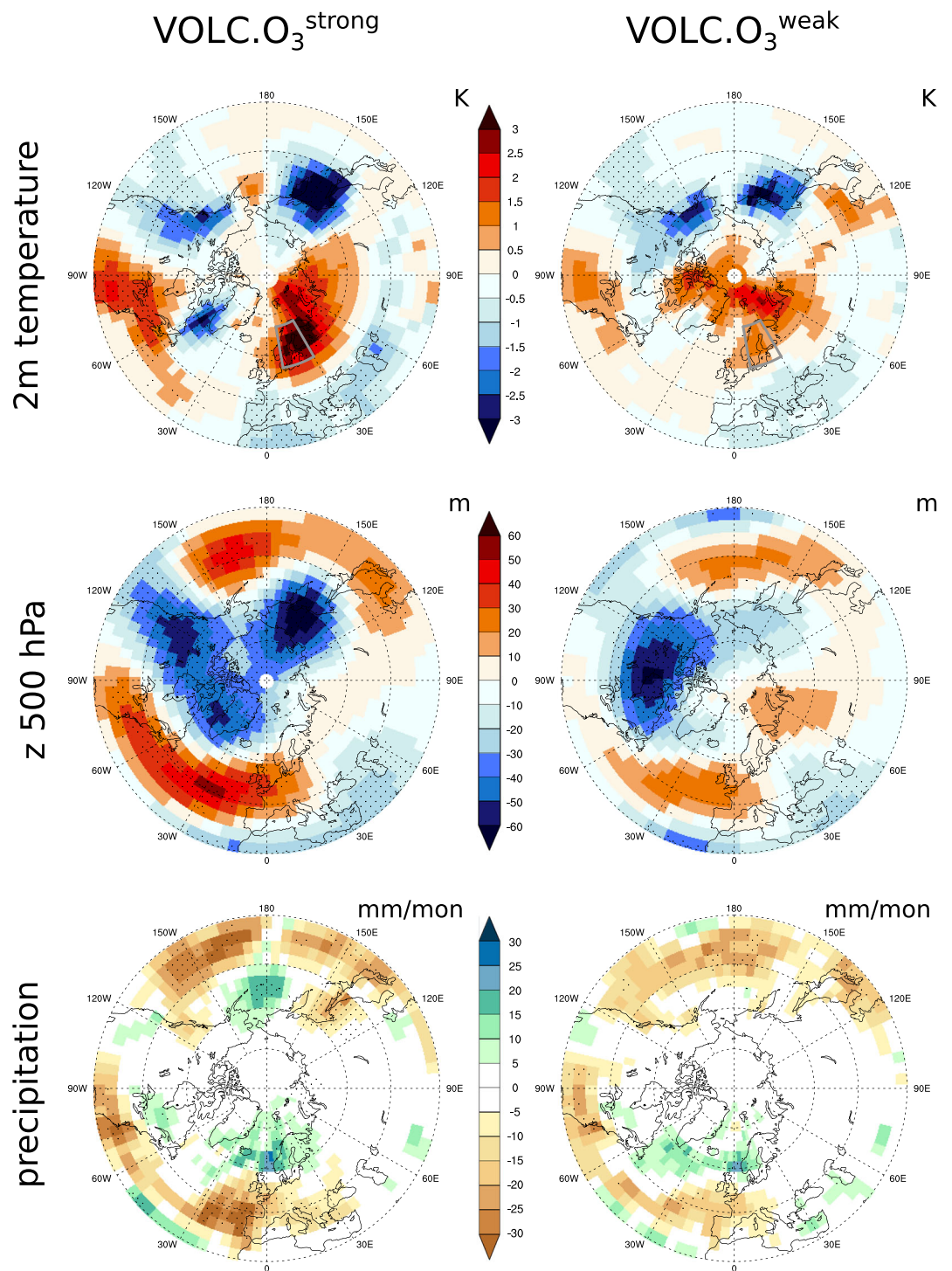


Figure 4. Ensemble mean anomalies for (top) the 2 m temperature, (middle) 500 hPa geopotential height, and (bottom) precipitation in the winter (DJF) following the eruption for the strong ozone gradient climatology (VOLC.O₃^{strong}, left) and the weak gradient climatology (VOLC.O₃^{weak}, right). Anomalies are expressed in terms of anomalies to the DJF mean in the corresponding control (CTRL.O₃^{strong} and CTRL.O₃^{weak}). Significant differences ($p \leq 0.05$, Student's t test) are indicated by stippling. Gray boxes in the temperature plots indicate the Scandinavian region used to calculate temperature anomalies.

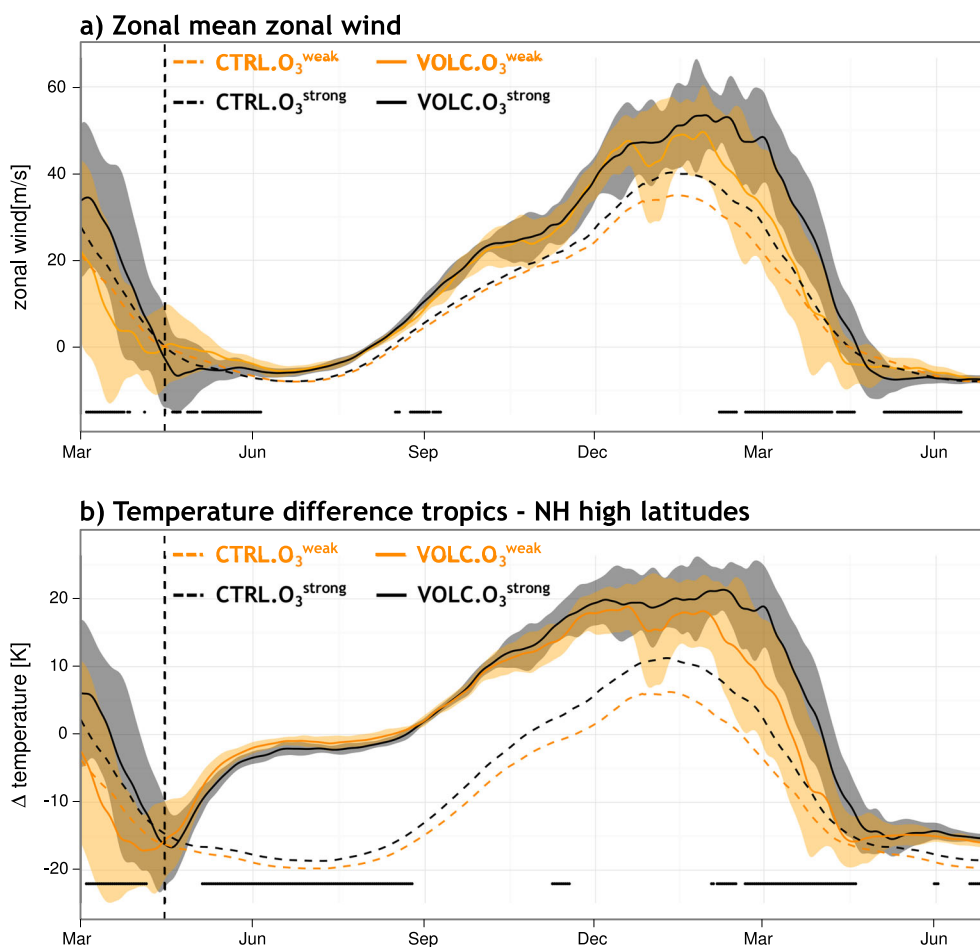


Figure 5. (a) Time series of the daily zonal mean zonal wind at 60°N (\bar{u}_{60}) and 10 hPa in m/s for VOLC.O₃^{strong} (solid black) and VOLC.O₃^{weak} (solid orange). (b) Daily zonal mean stratospheric temperature difference in K at 40 hPa between the tropics and the northern high latitudes (i.e., 20°S–20°N mean minus 70°N–90°N mean). Solid lines: ensemble mean. Shaded areas: ensemble standard deviation. Dashed lines: mean annual cycle in the control ensembles (black: CTRL.O₃^{strong}, orange: CTRL.O₃^{weak}). Vertical dashed line: start of the eruption. Dots at the bottom: significant differences between the two perturbed ensembles (Student's t test with $p \leq 0.05$). All time series are smoothed by a 11 day low-pass filter.

stronger in the simulation with larger ozone gradients in the middle stratosphere (VOLC.O₃^{strong}). Besides some weeks in April, the two control ensembles differ significantly ($p \leq 0.05$, Student's t test) during the entire year (not shown). In the winter season both control ensemble experiments lie within the uncertainty range (one standard deviation) of the daily average \bar{u}_{60} derived from ERA Interim (average 1979–2013, see supporting information Figure S3) [Dee *et al.*, 2011].

The different vortex intensities are explained by the differences in the ozone climatologies. In the O₃^{strong} climatology higher ozone concentrations are found in the lower and middle stratosphere, with larger anomalies in the tropical stratosphere than in the polar region (Figure 2a). Higher ozone values in the tropics lead to a more efficient UV absorption and thus to higher temperatures in the tropical lower stratosphere in the strong ozone gradient case. Since the temperature anomalies at the poles are smaller due to less insolation, the net effect is an increase of the temperature gradient between tropics and the northern high latitudes in the lower and middle stratosphere (Figure 2b). In both ensembles the intensity of the polar vortex is closely related to this temperature difference. In the stratosphere the correlation between \bar{u}_{60} and the meridional temperature difference between the tropics and high latitudes exceeds 0.95 at all levels between 10 hPa and 100 hPa. Consequently, the stratospheric temperature differences between the two control ensemble experiments are the driver for the differences in the vortex intensities [Andrews *et al.*, 1987].

In the perturbed ensemble experiment the stratospheric temperatures are also affected by the volcanic aerosol, whose highest concentrations are in the regions where the two ozone climatologies differ the

most (solid contours in Figure 2a). In these layers the volcanic aerosols are responsible for an increase of the absorption of near-infrared and infrared radiation, which leads to anomalous high temperatures, and alter the lower stratospheric temperature gradient between the tropics and the poles. For all ensembles, the temporal development of the temperature difference at 40 hPa is shown in Figure 5b. The 40 hPa level is selected, since the highest correlation coefficients ($r > 0.98$) between the temperature difference and the vortex index in the control ensembles are found at this altitude. However, the results at stratospheric levels above and below are comparable to the results at 40 hPa. The dashed lines in Figure 5b represent the mean annual cycle of the temperature gradients in the two control ensembles. The differences between the two cycles resemble the differences between the ozone climatologies. Relative to the control ensembles the temperature differences in VOLC.O₃^{strong} and VOLC.O₃^{weak} starts to increase immediately after the eruption and reaches its maximum in winter. In summer, intensifications are very similar (although with slightly higher wind speeds in VOLC.O₃^{weak}). From November to April, higher temperature differences are found in the ensemble with larger meridional ozone gradients (VOLC.O₃^{strong}). The meridional temperature profile for the perturbed and unperturbed DJF temperatures at 40 hPa is shown in Figure S4.

3.4. Stratosphere-Troposphere Coupling

In order to influence climate at the surface, stratospheric zonal wind anomalies have to propagate vertically through the tropopause. To illustrate the dynamic coupling between the stratosphere and the troposphere we show Hovmöller diagrams of both perturbed ensemble \bar{u}_{60} means relative to the corresponding control (Figure 6). The pattern is similar in both ensemble experiments. An intensification of the zonal mean zonal wind starts in the upper stratosphere about 2 months after the beginning of the eruption. In the following months the signal propagates downward into the lower stratosphere. However, the magnitude of anomalies in the lower stratosphere and the troposphere differs between the ensemble experiments showing higher anomalies in later winter in VOLC.O₃^{strong}. During the winter season, several pulses of downward propagating positive signals from the stratosphere to the troposphere are visible in the VOLC.O₃^{strong} ensemble average, whereas much fewer events are found in VOLC.O₃^{weak}. In the next step we show that these events, visible in the ensemble mean, are related to a larger number of stratosphere-troposphere couplings in the VOLC.O₃^{strong} ensemble.

3.5. Robustness Tests

The ensemble mean \bar{u}_{60} gives only hint on the coupling between the stratosphere and the troposphere, as information on the single events is partly lost by the averaging procedure. Furthermore, it could happen that a single ensemble member dominates the anomaly pattern shown in Figure 4 or 6. Therefore, we analyze the temperature anomalies and the stratosphere-troposphere couplings in detail.

For the Scandinavian surface temperature anomalies clear differences are found between the two ensemble experiments. The histogram for the posteruption DJF temperature anomalies averaged over northern Europe (10°E–30°E and 55°N–70°N, gray box in Figure 4) reveals that the majority of ensemble members in VOLC.O₃^{strong} are warmer than the average anomaly in VOLC.O₃^{weak} (Figure 7a). Therefore, the temperature anomalies shown in Figure 4 are not just dominated by one or two extreme members.

The same applies to the number of stratosphere-troposphere couplings. As a measure for the characterization of days with coupling events or anomalously high zonal winds in the troposphere and lower stratosphere, \bar{u}_{60} is averaged over the levels 1000 to 100 hPa. This measure does not directly consider the conditions at higher atmospheric levels. However, a composite over events with the index value exceeding a certain threshold (e.g., one standard deviation σ) reveals that anomalously high wind speeds in the lower levels are preceded by anomalously high wind conditions at higher levels in the stratosphere by up to 30 days (Figure 7b). This behavior is found in both control simulations, and also when higher thresholds are used. Applied to the posteruption winter of the perturbed simulations 123 days with anomalous high winds in the troposphere are found in the members of VOLC.O₃^{strong}, whereas only 57 days show stratosphere-troposphere couplings in the VOLC.O₃^{weak} simulations (using a threshold of $2 \cdot \sigma_{\text{CTRL.O}_3^{\text{strong}}}$). This result is again independent of the threshold applied as the comparison for threshold between 0.5 and 3.0 σ shows (Figure 7c). Finally, using a jackknife resampling test [von Storch and Zwiers, 2000] we test whether these results are dominated by a single extreme member. The number of days with a wind speed index $\geq 2 \cdot \sigma_{\text{CTRL.O}_3^{\text{strong}}}$ were calculated for all possible combinations, where one member was excluded from the statistics. The histogram of the results (Figure 7d) show that in any case, the two perturbed ensembles differ notably and reveal the robustness of the results.

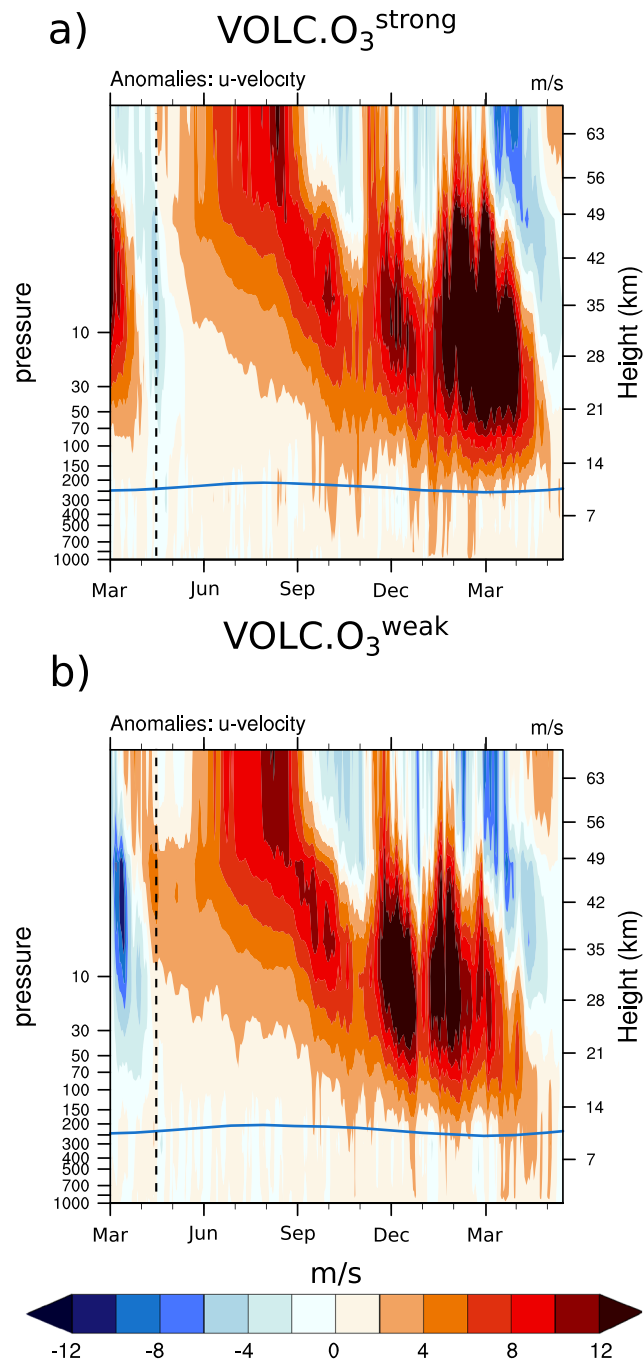


Figure 6. Ensemble mean daily zonal mean zonal wind anomalies in m/s at 60°N (\bar{u}_{60}) as a function of height and time, for (a) VOLC.O₃^{strong} and (b) VOLC.O₃^{weak}. The start of the eruption is indicated by the vertical dashed line. Anomalies are expressed relative to the corresponding ensemble mean. The thick blue line denotes the approximate tropopause height.

3.6. Nonlinearity

Finally, we address whether the impact of the two perturbations, the ozone climatology and the volcanic eruption, can be linearly superimposed. Again we use the mean tropospheric wind index defined above, but instead of anomalies with respect to the corresponding control ensemble sets, we consider the absolute values of the ensemble simulations. The effect of the ozone climatology is assessed using the control ensembles. The stronger gradient climatology leads to an intensification of the winter zonal winds of around 0.55 m/s in the mean value as well as in the higher percentiles. The effect of the eruption on the zonal wind extracted from the difference between CTRL.O₃^{weak} and VOLC.O₃^{weak} is 1.6 m/s for the mean and 5.2 m/s for

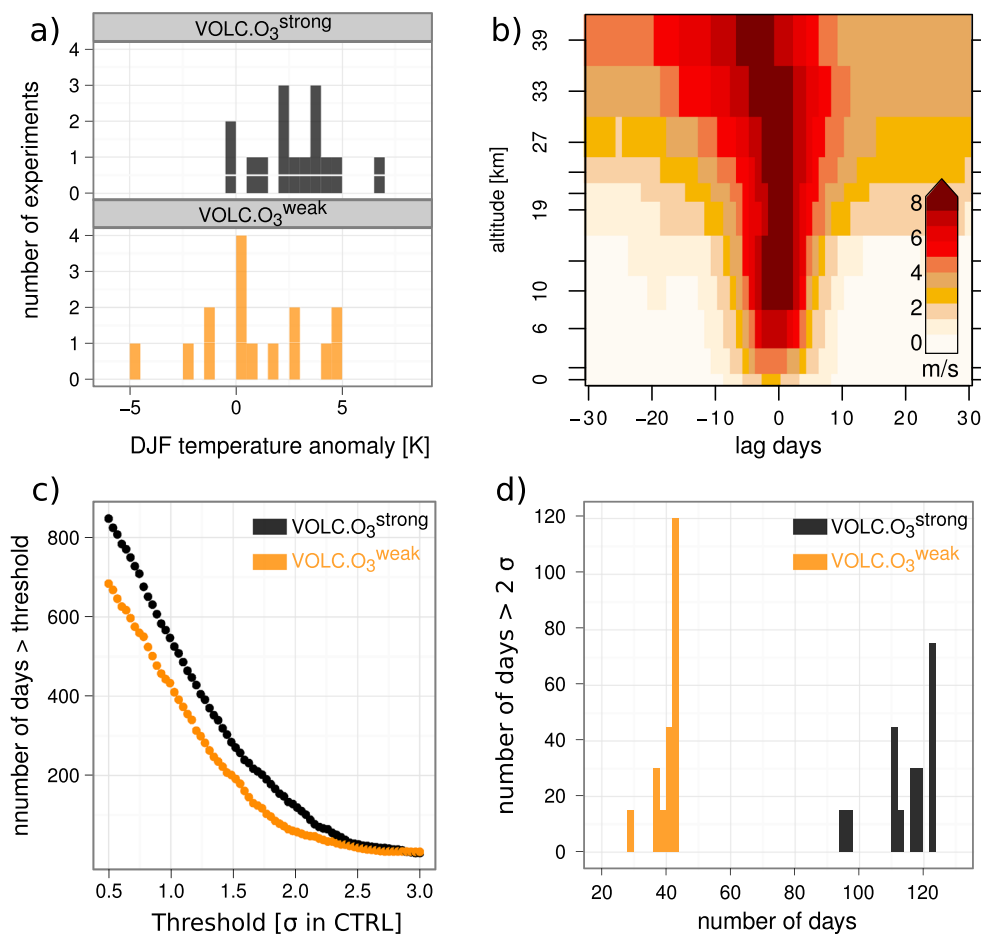


Figure 7. (a) Histogram for the post eruption northern Europe DJF temperature anomaly in the ensemble member. The temperature anomaly was averaged over the region 10°E–30°E and 55°N–70°N (binwidth of the histogram: 0.5 K). (b) Composite of the time–height development of anomalies in the zonal mean zonal wind at 60°N (\bar{u}_{60}) in m/s for events with anomalously high mean tropospheric wind speed. An event is defined as a day (for multiday events the central day was chosen), where the mean \bar{u}_{60} between 1000 and 100 hPa exceeds one standard deviation ($\sigma = 2.85$ m/s). The composite shows the temporal development for the 30 days before and after the exceeding of the threshold for CTRL.O₃^{strong} (based on 460 events). (c) Number of days in the posteruption winter season where the mean \bar{u}_{60} between 1000 and 100 hPa exceeds a given threshold (expressed as standard deviation in CTRL.O₃^{strong}, reaching from 0.5 to 3), for VOLC.O₃^{strong} and VOLC.O₃^{weak}, respectively. (d) Histogram (binwidth: 2 days) of the number of days with \bar{u}_{60} between 1000 and 100 hPa > 2 · σ using a leave-one-out jackknife test for both perturbed ensembles.

the 95th percentile. Assuming a linear superposition of both effects, the combined effect should result in an intensification of around 2.15 m/s for the mean value and 5.75 m/s for the 95th percentile. However, between CTRL.O₃^{weak} and VOLC.O₃^{strong} differences of 2.6 m/s for the mean value and 6.4 m/s for the 95th percentile are found, which indicates some nonlinear, amplifying coupling between the ozone differences and the volcanic signal.

4. Comparison With Data

When comparing the European winter warming pattern from both ensembles to the climate signals in reconstructions, the VOLC.O₃^{strong} ensemble is in better agreement. Fischer et al. [2007] reconstructed the average winter temperature, pressure, and precipitation response after 15 major volcanic eruptions based on multiproxy reconstructions for Europe. They found a clear and significant positive phase of the NAO with the corresponding temperature and precipitation pattern [Fischer et al., 2007, Figure 2]. Also the absolute values of the anomalies compare very well. However, given that the Tambora eruption simulated here is the strongest eruption of the last several hundred years and the Fischer et al. [2007] composite represents the average over 15 large volcanic eruptions a direct comparison of the absolute anomalies is difficult. Yet the high significance of the anomalies gives us confidence that the model response is robust compared to what we expect from the reconstructions.

It should be noted that the setup used in this study does not simulate the interactive response of the chemistry to the tropical eruption. With interactive ozone chemistry the response may be different due to positive or negative feedbacks. In the preindustrial case, without ozone-depleting substances (ODS) ozone values are expected to increase in the extratropical lower stratosphere, due to the deactivation of NO_x via heterogeneous reactions on the surface of the volcanic aerosols [Tie and Brasseur, 1995; Solomon *et al.*, 1996; Anet *et al.*, 2013]. This effect may reduce the meridional ozone gradient and weaken the dynamic response.

With ODS in the stratosphere, ozone values are reduced in the extratropical lower stratosphere by the activation of chlorine and the resulting ozone destruction [Tie and Brasseur, 1995; Kinne *et al.*, 1992; Rozanov *et al.*, 2002]. In this case the eruption might increase the meridional ozone gradient and amplify the dynamic effects. Furthermore, the cooling of the polar stratosphere that accompanies the vortex intensification can increase the number of polar stratospheric clouds, further reduce ozone, and create a positive feedback.

The ozone climatologies used in this sensitivity study originate from two different sources. The weak gradient climatology is based on observational data for the late 20th century. The second climatology with stronger meridional gradients was extracted from a preindustrial control simulation with interactive chemistry. Although each climatology represents a distinct state of the stratosphere (preindustrial without ozone depletion versus present day with ozone depletion), a direct interpretation of the results in terms of a shift from preindustrial to present day is not possible due to the different data sources and biases (see Stenke *et al.* [2013] for an evaluation of the chemistry climate model).

Nevertheless, the two climatologies are compared to existing transient data sets to estimate how the forcings used in this sensitivity study compare to ozone changes in the past and to the uncertainties between different ozone reconstructions. The knowledge of the preindustrial (1600 A.D. in this study) ozone values is of course limited and based only on model results. However, since the emission of ozone-depleting substances is a phenomena of the late 20th century, we safely assume that ozone values of the early 20th century are comparable to preindustrial values [Brönnimann *et al.*, 2003].

In the last years, a few data sets of transient ozone concentrations were developed. For the CMIP5 simulations, Cionni *et al.* [2011] created ozone forcing from 1850 onward based on model results and observations Stratosphere-troposphere Processes And their Role in Climate (SPARC). Due to the approach they used, the variability in the early decades of the record is rather low. Therefore, we also compare to a newer ozone reconstruction of Brönnimann *et al.* [2013] that starts in 1900 and show realistic interannual variability (HISTOZ 1.0). The latter reconstruction is based on SOCOL (version 2) simulations [Fischer *et al.*, 2008], augmented by historical total ozone observations from the 1920s to 1970s. From 1979 it is supplemented with an observation-based ozone data set [Hassler *et al.*, 2008].

Two periods were selected for the comparison. An early period from 1900 to 1919 represents the undisturbed situation, i.e., without the attendance of ODS in the atmosphere, and a later period ranging from 1970 to 1989 (roughly the period of Fortuin and Kelder [1998]) that includes the effect of ozone depletion. All values are averaged over the winter season (DJF). With ODS the climatology of Fortuin and Kelder [1998] compares very well with the SPARC record, which is expected since this climatology is one of the data sources used to compile the SPARC climatology. Substantial differences between HISTOZ (which for the majority of the period consists of the [Hassler *et al.*, 2008] observation data set) and SPARC are found for the meridional gradient, with HISTOZ showing stronger gradients at 10 and 20 hPa and weaker gradients at 50 hPa (Figure 8, left). Without ODS the deviations between the different data sets become larger. Again HISTOZ (which in this period is based on SOCOL simulations only, see Fischer *et al.* [2008]) is characterized by larger meridional ozone differences at 10 and 20 hPa and weaker differences at 50 hPa (Figure 8, middle).

The important comparison is the change in the ozone profile caused by ODS (Figure 8, right). Here we find substantial differences to SPARC and HISTOZ, which confirms our statement that the results should not be interpreted as a shift from preindustrial to present day. At 10 and 20 hPa we find a clear ozone reduction in the tropics in our climatology whereas the two transient records show either a weak reduction (HISTOZ) or slight increase (SPARC) in the tropics and a clear decrease of the ozone values in the northern high latitudes. The effect of ozone depletion on the meridional ozone gradient is therefore much stronger (compared to HISTOZ) or even the opposite (SPARC). At 50 hPa a general ozone reduction with the attendance of ODS is found on nearly all latitudes in all data sets. However, the reductions are between 2 and 4 times higher in the climatologies used in this study.

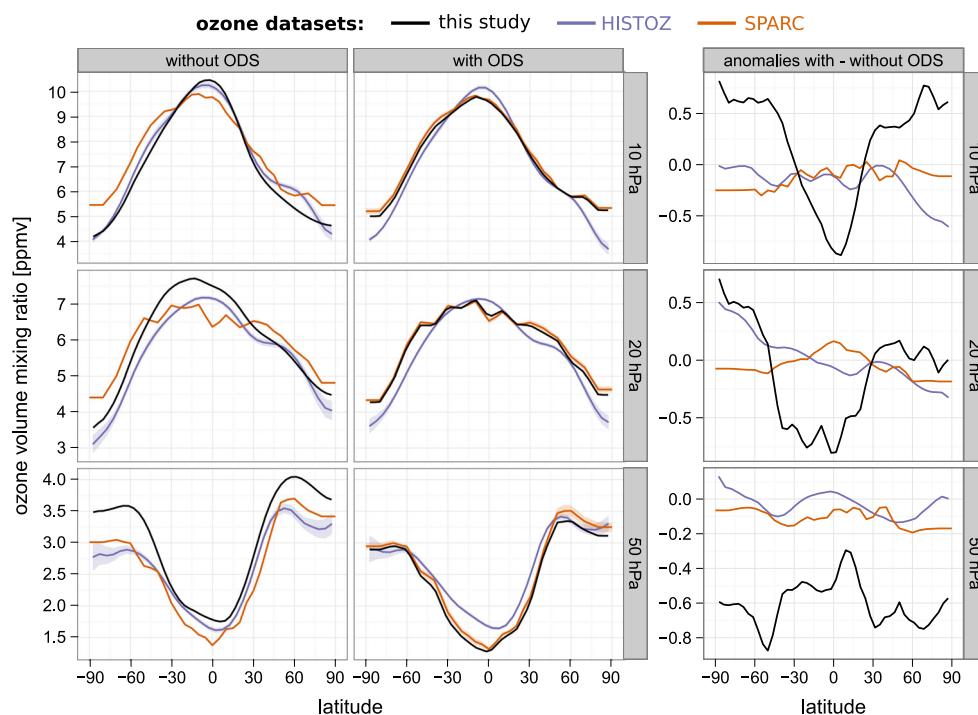


Figure 8. Comparison between the DJF ozone volume mixing ratios (ppmv) in the climatologies used in this study to the HISTOZ 1.0 [Brönnimann *et al.*, 2013] and the SPARC data set [Cionni *et al.*, 2011]. (left) Mean ozone profile for periods without ODS (average 1900–1919). (middle) Profile for periods with the attendance of ODS (average 1970–1989). (right) Change in the ozone mixing ratios between the two periods. Meridional profiles are shown for the 10, 20, and 50 hPa altitudes. Shading indicates one standard deviation in the corresponding record. Please note the different axis scaling.

5. Discussion and Conclusions

In ensemble sensitivity simulations forced with two different ozone climatologies, we found a strong difference in the coupling of positive wind speed anomalies after large volcanic eruptions from the stratosphere to the troposphere. These differences are related to the different background states of the stratosphere linked to the two ozone climatologies. The two ozone climatologies mainly differ in the meridional ozone gradients between high and low latitudes. With a larger ozone gradient the northern winter polar vortex is around 15% stronger, and the volcanic eruption causes an additional intensification of the vortex. Although the volcanic intensification is roughly of similar strength in the weak gradient ensemble (VOLC.O₃^{weak}), the combined net effect is larger in VOLC.O₃^{strong} and results in a higher number of stratosphere-troposphere coupling events which lead to higher and more extended temperature anomalies in northern Europe.

This analysis is subjected to a number of caveats and limitations which we discuss in the following:

1. The volcanic forcing by Arfeuille *et al.* [2013a] that is used in this study to implement the impact of the Tambora eruptions disagrees in some aspects with earlier volcanic forcing reconstructions. In particular the high asymmetry, with the majority of aerosols spread into the Southern Hemisphere, is discussed. An explanation for this asymmetry is already given by the authors. Tambora erupted in April 1815, corresponding to the fall season of the Southern Hemisphere. In the following weeks and months the aerosol accumulated in the tropical stratosphere and was slowly transported toward higher latitudes. In the stratosphere the transport is mainly directed toward the winter hemisphere [Holton *et al.*, 1995], which explains the larger accumulation of aerosols in the Southern Hemisphere. This is also in agreement with transport assumptions made by [Ammann *et al.*, 2003] for their volcanic forcing. A similar, although less pronounced asymmetry, can be found in the forcing of Crowley *et al.* [2008]. Moreover, as shown in Arfeuille *et al.* [2013b], the methodology used succeeds in reproducing the very asymmetric aerosol cloud of the Agung 1963 eruption, which has a similar timing and location compared to the Tambora 1815 eruption (i.e., March, 8°S) and a similar asymmetric hemispheric partitioning [Stothers, 2001]. Another caveat related to the volcanic forcing is that the forcing was calculated offline and therefore does not react to the

different dynamics related to the different ozone climatologies. However, this approach is chosen in most of the GCMs today.

2. The simulated heating in the tropical stratosphere forced by the volcanic aerosols is probably overestimated, a feature that is common to many GCMs [Lanzante and Free, 2008; Driscoll et al., 2012]. A part of the overestimation may be related to the fact that the chosen setup does not simulate the ozone chemistry interactively and therefore the cooling effect caused by tropical ozone depletion is not included [Kirchner et al., 1999; Stenchikov et al., 2002].
3. This study does not consider the effect of different QBO phases on the results, instead all ensembles are nudged toward the same, easterly QBO phase in the winter after the eruption. Since the northern high-latitude geopotential height in the stratosphere is known to be in general higher during easterly phases of the QBO [Holton and Tan, 1980, 1982], the vortex intensification may be even stronger when the QBO is in a westerly phase [Stenchikov et al., 2004; Thomas et al., 2009a]. In which way, this affects the anomalies at the surface needs to be assessed in future work.

In the IPCC AR4, several models used a constant ozone climatology [Miller et al., 2006; Son et al., 2010] and it was found that the winter warming pattern is in general too weak compared with observations [Miller et al., 2006; Stenchikov et al., 2006]. Beginning with CMIP5 a prescribed time-dependent ozone forcing, which considers changes in the atmospheric ozone composition is recommended, but the models still fail in reproducing an appropriate winter warming response [Driscoll et al., 2012].

A part this failure may be related to the fact that the effect of ozone depletion, as observed after Pinatubo, are still not considered in the forcing [Cionni et al., 2011]. The polar ozone depletion might strengthen the positive AO phase [Stenchikov et al., 2002]. However, even with prescribed ozone anomalies models still fail in producing a significant winter warming pattern, even in larger ensembles [Thomas et al., 2009b]. Furthermore, winter warming patterns have also been found for eruptions that were not influenced by the effect of ozone-depleting substances, i.e., eruption before 1970.

The results presented here show that the state of the stratosphere, especially the polar vortex, is an important prerequisite for a decent simulation of the dynamic response to eruptions and that the meridional ozone gradient strongly influences the state of the polar vortex.

The differences between existing ozone records for the past and the uncertainties in chemistry-climate model-based ozone projections for the future [Eyring et al., 2007; Karpechko and Gillett, 2010] are large. We show that the decision for a particular ozone data set might significantly influence the dynamic response to tropical volcanic eruptions in a nonlinear way. Analyzing the mechanisms involved in the stratosphere-troposphere coupling was out of scope of this sensitivity study. However, understanding which processes are dominant (compare Gerber et al. [2012]) is necessary for a thorough evaluation of the role of ozone gradients. Furthermore, the evidence presented here needs to be evaluated in other GCMs without interactive ozone chemistry and with other volcanic eruptions. Future work will also assess the question how the findings change with interactive ozone chemistry.

Acknowledgments

The authors thank the three anonymous reviewers for their fruitful comments. Moreover, we would like to thank Greg Bodeker (Bodeker Scientific) and Birgit Hassler (NOAA) for providing the combined vertical ozone profile database through the British Atmospheric Data Centre (BADC). This project is supported by the Swiss National Science Foundation under the grant CRS1122-130642 (FUPSOL). This paper profited from discussions during the PAGES/FUSOL Workshop in 2012.

References

- Ammann, C. M., G. A. Meehl, W. M. Washington, and C. S. Zender (2003), A monthly and latitudinally varying volcanic forcing dataset in simulations of 20th century climate, *Geophys. Res. Lett.*, *30*(12), 1–4, doi:10.1029/2003GL016875.
- Andrews, D. G., J. R. Holton, and C. B. Leovy (1987), *Middle Atmosphere Dynamics*, 489 p., Academic Press, London.
- Anet, J. G., et al. (2013), Forcing of stratospheric chemistry and dynamics during the Dalton Minimum, *Atmos. Chem. Phys.*, *13*, 10,951–10,967, doi:10.5194/acp-13-10951-2013.
- Arfeuille, F., D. Weisenstein, H. Mack, E. Rozanov, T. Peter, and S. Brönnimann (2013a), Volcanic forcing for climate modeling: A new microphysics-based dataset covering years 1600–present, *Clim. Past Discuss.*, *9*, 967–1012, doi:10.5194/cpd-9-967-2013.
- Arfeuille, F., B. P. Luo, P. Heckendorn, D. Weisenstein, J. X. Sheng, E. Rozanov, M. Schraner, S. Brönnimann, L. W. Thomason, and T. Peter (2013b), Modeling the stratospheric warming following the Mt. Pinatubo eruption: Uncertainties in aerosol extinctions, *Atmos. Chem. Phys.*, *13*, 11,221–11,234, doi:10.5194/acp-13-11221-2013.
- Auchmann, R., S. Brönnimann, L. Breda, M. Bühler, R. Spadin, and A. Stickler (2012), Extreme climate, not extreme weather: The summer of 1816 in Geneva, Switzerland, *Clim. Past*, *8*, 325–335, doi:10.5194/cp-8-325-2012.
- Baldwin, M. P., and T. J. Dunkerton (2001), Stratospheric harbingers of anomalous weather regimes, *Science*, *294*(5542), 581–4, doi:10.1126/science.063315.
- Baldwin, M. P., X. Cheng, and T. J. Dunkerton (1994), Observed correlations between winter-mean tropospheric and stratospheric circulation anomalies, *Geophys. Res. Lett.*, *21*(12), 1141–1144.
- Baldwin, M. P., M. Dameris, and T. G. Shepherd (2007), How will the stratosphere affect climate change?, *Science*, *316*, 1576–1577.
- Brönnimann, S., J. Staehelin, S. F. G. Farmer, J. C. Cain, T. Svendby, and T. Svenøe (2003), Total ozone observations prior to the IGY. I: A history, *Q. J. Roy. Meteorol. Soc.*, *129*(593), 2797–2817, doi:10.1256/qj.02.118.

- Brönnimann, S., J. L. Annis, C. Vogler, and P. D. Jones (2007), Reconstructing the quasi-biennial oscillation back to the early 1900s, *Geophys. Res. Lett.*, *34*, L22805, doi:10.1029/2007GL031354.
- Brönnimann, S., J. Bhend, J. Franke, S. Flückiger, A. M. Fischer, R. Bleisch, G. Bodeker, B. Hassler, E. Rozanov, and M. Schraner (2013), A global historical ozone data set and prominent features of stratospheric variability prior to 1979, *Atmos. Chem. Phys.*, *13*, 9623–9639, doi:10.5194/acp-13-9623-2013.
- Budich, R., M. Gioretta, J. Jungclaus, R. Redler, and C. Reick (2010), The MPI-M Millennium Earth System Model: An assembling guide for the COSMOS configuration, *MPI report*, Max-Planck Institute for Meteorology, Hamburg, Germany.
- Christiansen, B. (2001), Downward propagation of zonal mean zonal wind anomalies from the stratosphere to the troposphere: Model and reanalysis, *J. Geophys. Res.*, *106*(D21), 27,307–27,322, doi:10.1029/2000JD000214.
- Christiansen, B. (2005), Downward propagation and statistical forecast of the near-surface weather, *J. Geophys. Res.*, *110*, D14104, doi:10.1029/2004JD005431.
- Christiansen, B. (2008), Volcanic eruptions, large-scale modes in the Northern Hemisphere, and the El Niño–Southern Oscillation, *J. Climate*, *21*, 910–922, doi:10.1175/2007JCLI1657.1.
- Cionni, I., V. Eyring, J. F. Lamarque, W. J. Randel, D. S. Stevenson, F. Wu, G. E. Bodeker, T. G. Shepherd, D. T. Shindell, and D. W. Waugh (2011), Ozone database in support of CMIP5 simulations: Results and corresponding radiative forcing, *Atmos. Chem. Phys.*, *11*, 11,267–11,292, doi:10.5194/acp-11-11267-2011.
- Cole-Dai, J. (2010), Volcanoes and climate, *WIREs Clim. Change*, *1*, 824–839, doi:10.1002/wcc.76.
- Crowley, T., G. Zielinski, B. Vinther, R. Udisti, K. Kreutz, J. Cole-Dai, and E. Castellano (2008), Volcanism and the little ice age, *PAGES News*, *16*, 22–23.
- Dee, D. P., et al. (2011), The ERA-Interim reanalysis: Configuration and performance of the data assimilation system, *Q. J. Roy. Meteorol. Soc.*, *137*, 553–597, doi:10.1002/qj.828.
- Driscoll, S., A. Bozzo, L. J. Gray, A. Robock, and G. Stenchikov (2012), Coupled Model Intercomparison Project 5 (CMIP5) simulations of climate following volcanic eruptions, *J. Geophys. Res.*, *117*, D17105, doi:10.1029/2012JD017607.
- Eyring, V., et al. (2007), Multimodel projections of stratospheric ozone in the 21st century, *J. Geophys. Res.*, *112*, D16303, doi:10.1029/2006JD008332.
- Fischer, A. M., et al. (2008), Interannual-to-decadal variability of the stratosphere during the 20th century: Ensemble simulations with a chemistry-climate model, *Atmos. Chem. Phys.*, *8*, 7755–7777, doi:10.5194/acp-8-7755-2008.
- Fischer, E. M., J. Luterbacher, E. Zorita, S. F. B. Tett, C. Casty, and H. Wanner (2007), European climate response to tropical volcanic eruptions over the last half millennium, *Geophys. Res. Lett.*, *34*, 1–6, doi:10.1029/2006GL027992.
- Fortuin, J. P. F., and H. Kelder (1998), An ozone climatology based on ozonesonde and satellite measurements, *J. Geophys. Res.*, *103*, 31,709–31,734, doi:10.1029/1998JD200008.
- Gerber, E. P., et al. (2012), Assessing and understanding the impact of stratospheric dynamics and variability on the Earth system, *Bull. Am. Meteorol. Soc.*, *93*, 845–859, doi:10.1175/bams-d-11-00145.1.
- Gillett, N. P., and D. W. J. Thompson (2003), Simulation of recent Southern Hemisphere climate change, *Science*, *302*(5643), 273–275, doi:10.1126/science.1.087440.
- Gillett, N. P., M. R. Allen, R. E. Mcdonald, C. A. Senior, D. T. Shindell, and G. A. Schmidt (2002), How linear is the Arctic Oscillation response to greenhouse gases?, *J. Geophys. Res.*, *107*, 1–7, doi:10.1029/2001JD000589.
- Graf, H. F., I. Kirchner, A. Robock, and I. Schult (1993), Pinatubo eruption winter climate effects: Model versus observations, *Clim. Dynam.*, *92*, 81–93.
- Hagemann, S. (2002), An improved land surface parameter dataset for global and regional climate models, *MPI report 336*, Max-Planck Institut fuer Meteorologie, Hamburg, Germany.
- Hassler, B., G. E. Bodeker, and M. Dameris (2008), Technical note: A new global database of trace gases and aerosols from multiple sources of high vertical resolution measurements, *Atmos. Chem. Phys.*, *8*, 5403–5421, doi:10.5194/acp-8-5403-2008.
- Hurrell, J. W. (1995), Decadal trends in the North Atlantic Oscillation: Regional temperatures and precipitation, *Science*, *269*, 676–679.
- Holton, J. R., and H.-C. Tan (1980), The influence of the equatorial-biennial oscillation on the global circulation at 50 mb, *J. Atmos. Sci.*, *37*, 2200–2208.
- Holton, J. R., and H.-C. Tan (1982), The quasi-biennial Northern Hemisphere Oscillation in the lower stratosphere, *J. Meteorol. Soc. Jpn.*, *60*(1), 140–148.
- Holton, J. R., P. H. Haynes, M. E. McIntyre, A. R. Douglass, R. B. Rood, and L. Pfister (1995), Stratosphere–troposphere exchange, *Rev. Geophys.*, *33*(4), 403–439.
- Jungclaus, J. H., N. Keenlyside, M. Botzet, H. Haak, J.-J. Luo, M. Latif, J. Marotzke, U. Mikolajewicz, and E. Roeckner (2006), Ocean circulation and tropical variability in the coupled model ECHAM5/MPI-OM, *J. Climate*, *19*, 3952–3972, doi:10.1175/JCLI3827.1.
- Jungclaus, J. H., et al. (2010), Climate and carbon-cycle variability over the last millennium, *Clim. Past*, *6*, 723–737, doi:10.5194/cp-6-723-2010.
- Karpechko, A. Y., and N. P. Gillett (2010), Quantitative assessment of Southern Hemisphere ozone in chemistry-climate model simulations, *Atmos. Chem. Phys.*, *10*, 1385–1400.
- Kinne, S., O. B. Toon, and M. J. Prather (1992), Buffering of stratospheric circulation by changing amounts of tropical ozone a Pinatubo case study, *Geophys. Res. Lett.*, *19*(19), 1927–1930.
- Kirchner, I., G. L. Stenchikov, H.-F. Graf, A. Robock, and J. C. Antuña (1999), Climate model simulation of winter warming and summer cooling following the 1991 Mount Pinatubo volcanic eruption, *J. Geophys. Res.*, *104*(D16), 19,039–19,055, doi:10.1029/1999JD900213.
- Kodera, K. (1994), Influence of volcanic eruptions on the troposphere through stratospheric dynamical processes in the Northern Hemisphere winter, *J. Geophys. Res.*, *99*(D1), 1273–1282.
- Lanzante, J. R., and M. Free (2008), Comparison of radiosonde and GCM vertical temperature trend profiles: Effects of dataset choice and data homogenization, *J. Climate*, *21*, 5417–5435, doi:10.1175/2008JCLI2287.1.
- Marsland, S. (2003), The Max-Planck-Institute global ocean/sea ice model with orthogonal curvilinear coordinates, *Ocean Model.*, *5*(2), 91–127, doi:10.1016/S1463-5003(02)00015-X.
- Miller, R. L., G. A. Schmidt, and D. T. Shindell (2006), Forced annular variations in the 20th century Intergovernmental Panel on Climate Change Fourth Assessment Report models, *J. Geophys. Res.*, *111*, 1–17, doi:10.1029/2005JD006323.
- Pinto, J. G., and C. C. Raible (2012), Past and recent changes in the North Atlantic Oscillation, *WIREs Clim. Change*, *3*, 79–90, doi:10.1002/wcc.150.
- Raible, C. C., U. Luksch, and K. Fraedrich (2004), Precipitation and Northern Hemisphere regimes, *Atmos. Sci. Lett.*, *5*, 43–55, doi:10.1016/j.atmoscilet.2003.12.001.
- Robock, A. (2000), Volcanic eruptions and climate, *Rev. Geophys.*, *38*, 191–219.

- Robock, A., and J. Mao (1992), Winter warming from large volcanic eruptions, *Geophys. Res. Lett.*, *12*, 2405–2408.
- Roeckner, E., et al. (2003), The atmospheric general circulation model ECHAM5 - Model description, *MPI report 349*, Max-Planck Institute for Meteorology, Hamburg, Germany.
- Roazanov, E. V., M. E. Schlesinger, N. G. Andronova, F. Yang, S. L. Malyshev, V. A. Zubov, T. A. Egorova, and B. Li (2002), Climate/chemistry effects of the Pinatubo volcanic eruption simulated by the UIUC stratosphere/troposphere GCM with interactive photochemistry, *J. Geophys. Res.*, *107*(D21), 4594, doi:10.1029/2001JD000974.
- Shepherd, T. G. (2002), Issues in stratosphere-troposphere coupling, *J. Meteorol. Soc. Jpn.*, *80*(4B), 769–792, doi:10.2151/jmsj.80.769.
- Shindell, D. T., G. A. Schmidt, M. E. Mann, and G. Faluvegi (2004), Dynamic winter climate response to large tropical volcanic eruptions since 1600, *J. Geophys. Res.*, *109*, D05104, doi:10.1029/2003JD004151.
- Solomon, S. (1999), Stratospheric ozone depletion: A review of concepts and history, *Rev. Geophys.*, *37*(3), 275–316, doi:10.1029/1999RG900008.
- Solomon, S., R. W. Portmann, R. R. Garcia, L. W. Thomason, L. R. Poole, M. P. McCormick, and C. Cly (1996), The role of aerosol variations in anthropogenic ozone depletion at northern midlatitudes, *J. Geophys. Res.*, *101*(95), 6713–6727.
- Son, S.-W., et al. (2010), Impact of stratospheric ozone on Southern Hemisphere circulation change: A multimodel assessment, *J. Geophys. Res.*, *115*, D00M07, doi:10.1029/2010JD014271.
- Song, Y., and W. A. Robinson (2004), Dynamical mechanisms for stratospheric influences on the troposphere, *J. Atmos. Sci.*, *61*, 1711–1725, doi:10.1175/1520-0469(2004)061<1711:DMFSIO>2.0.CO;2.
- Stenchikov, G., A. Robock, V. Ramaswamy, M. D. Schwarzkopf, K. Hamilton, and S. Ramchandran (2002), Arctic Oscillation response to the 1991 Mount Pinatubo eruption: Effects of volcanic aerosols and ozone depletion, *J. Geophys. Res.*, *107*(D24), 1–16, doi:10.1029/2002JD002090.
- Stenchikov, G., K. Hamilton, A. Robock, V. Ramaswamy, and M. D. Schwarzkopf (2004), Arctic Oscillation response to the 1991 Pinatubo eruption in the SKYHI general circulation model with a realistic quasi-biennial oscillation, *J. Geophys. Res.*, *109*, D03112, doi:10.1029/2003JD003699.
- Stenchikov, G., K. Hamilton, R. J. Stouffer, A. Robock, V. Ramaswamy, B. Santer, and H.-F. Graf (2006), Arctic Oscillation response to volcanic eruptions in the IPCC AR4 climate models, *J. Geophys. Res.*, *111*, 1–17, doi:10.1029/2005JD006286.
- Stenke, A., M. Schraner, E. Rozanov, T. Egorova, B. Luo, and T. Peter (2013), The SOCOL version 3.0 chemistry-climate model: Description, evaluation, and implications from an advanced transport algorithm, *Geosci. Model Dev.*, *6*, 1407–1427, doi:10.5194/gmd-6-1407-2013.
- Stothers, R. B. (1984), The great Tambora eruption in 1815 and its aftermath, *Science*, *224*(4654), 1191–1198.
- Stothers, R. B. (2001), Major optical depth perturbations to the stratosphere from volcanic eruptions: Stellar extinction period, 1961–1978, *J. Geophys. Res.*, *106*(D3), 2993–3003, doi:10.1029/2000JD900652.
- Taylor, K. E., R. J. Stouffer, and G. A. Meehl (2012), An overview of CMIP5 and the experiment design, *Bull. Am. Meteorol. Soc.*, *93*, 485–498, doi:10.1175/BAMS-D-11-00094.1.
- Thomas, M. A., M. A. Giorgetta, C. Timmreck, H.-F. Graf, and G. Stenchikov (2009a), Simulation of the climate impact of Mt. Pinatubo eruption using ECHAM5—Part 2: Sensitivity to the phase of the QBO, *Atmos. Chem. Phys.*, *9*, 3001–3009, doi:10.5194/acp-9-3001-2009.
- Thomas, M. A., C. Timmreck, M. a. Giorgetta, H.-F. Graf, and G. Stenchikov (2009b), Simulation of the climate impact of Mt. Pinatubo eruption using ECHAM5—Part 1: Sensitivity to the modes of atmospheric circulation and boundary conditions, *Atmos. Chem. Phys.*, *9*, 757–769, doi:10.5194/acp-9-757-2009.
- Thompson, D. W. J., M. P. Baldwin, and S. Solomon (2005), Stratosphere-troposphere coupling in the Southern Hemisphere, *J. Atmos. Sci.*, *62*, 708–715.
- Thompson, D. W. J., J. C. Furtado, and T. G. Shepherd (2006), On the tropospheric response to anomalous stratospheric wave drag and radiative heating, *J. Atmos. Sci.*, *63*, 2616–2629.
- Thompson, D. W. J., S. Solomon, P. J. Kushner, M. H. England, K. M. Grise, and D. J. Karoly (2011), Signatures of the Antarctic ozone hole in Southern Hemisphere surface climate change, *Nat. Geosci.*, *4*, 741–749, doi:10.1038/ngeo1296.
- Thompson, D. W. J., D. J. Seidel, W. J. Randel, C.-Z. Zou, A. H. Butler, C. Mears, A. Osso, C. Long, and R. Lin (2012), The mystery of recent stratospheric temperature trends, *Nature*, *491*, 692–697, doi:10.1038/nature11579.
- Tie, X., and G. Brasseur (1995), The response of stratospheric ozone to volcanic eruptions: Sensitivity to atmospheric chlorine loading, *Geophys. Res. Lett.*, *22*(22), 3035–3038.
- Timmreck, C. (2012), Modeling the climatic effects of large explosive volcanic eruptions, *WIREs Clim. Change*, *3*, 545–564, doi:10.1002/wcc.192.
- Valcke, S. (2013), The OASIS3 coupler: A European climate modelling community software, *Geosci. Model Dev.*, *6*, 373–388, doi:10.5194/gmd-6-373-2013.
- von Storch, H., and F. W. Zwiers (2000), *Statistical Analysis in Climate Research*, 484 p., Cambridge Univ. Press, Cambridge.
- Zanchettin, D., C. Timmreck, O. Bothe, S. J. Lorenz, G. Hegerl, H.-F. Graf, J. Luterbacher, and J. H. Jungclaus (2012), Delayed winter warming: A robust decadal response to strong tropical volcanic eruptions?, *Geophys. Res. Lett.*, *40*, 204–209, doi:10.1029/2012GL054403.
- Zhang, D., R. Blender, and K. Fraedrich (2012), Volcanoes and ENSO in millennium simulations: Global impacts and regional reconstructions in East Asia, *Theor. Appl. Climatol.*, *111*, 437–454, doi:10.1007/s00704-012-0670-6.